Ion energy distributions in laser-produced plasmas with two collinear pulses

2012 Plasma Sources Sci. Technol. 21 015016

(http://iopscience.iop.org/0963-0252/21/1/015016)

Plasma Sources Sci. Technol. **21** (2012) 015016 (10pp) doi:10.1088/0963-0252/21/1/015016

Ion energy distributions in laser-produced plasmas with two collinear pulses

Jon I Apiñaniz[1], Francisco J Gordillo-Vázquez[2] and Roberto Martínez[3]

[1] Dpto. Química Física, Universidad del País Vasco UPV/EHU, Facultad de Ciencia y Tecnología. Barrio Sarriena s/n, 48940 Leioa (Vizcaya), Spain
[2] Instituto de Astrofísica de Andalucía IAA, CSIC, Glorieta de la Astronomía s/n, 18080 Granada, Spain
[3] Dpto. Química Física, Universidad del País Vasco UPV/EHU, Facultad de Farmacia, Paseo de la Universidad, 7. 01006 Vitoria-Gasteiz (Alava), Spain

E-mail: r.martinez@ehu.es

Received 4 July 2011, in final form 21 December 2011
Published 2 February 2012
Online at stacks.iop.org/PSST/21/015016

Abstract
The formation and expansion dynamics of laser-produced plasmas was studied by means of the effect of a second delayed laser pulse upon the ion kinetic energy of the plasma created by the first one. Two types of measurements were carried out: ion kinetic energy distributions and overall ion time of flight (t.o.f.). Ion energy distributions were obtained with an electrostatic energy analyser, which allowed the observation of the energy distributions of each charge state separately while the ion t.o.f. signal was measured with an ion probe. Laser power densities ranged from 2×10^8 to 2×10^9 W cm^{-2} with 532 nm photons, and studies were extended to Al, Cu and Co targets. The effects of the second laser pulse on the plasma created by the first were very different depending on the interpulse delay. At low delays (from 0 to 10 ns) the second pulse produced an increase of the plasma average charge state and the maximum ion kinetic energy, while at higher delays (>20 ns) it produced a strong enhancement on the low charge yield (especially the single-charge ions) leaving unaltered the energies and yields of the high charges. An analysis of variations in both ion yield and kinetic energy produced interesting results regarding fundamental understanding of plasma formation and expansion dynamics, as well as possible improvements in technological applications based on laser-produced plasmas.

(Some figures may appear in colour only in the online journal)

1. Introduction

The physics of laser-produced plasmas involves different processes taking part in different phases and time scales [1]. In order to improve the knowledge about the mechanisms involved, researchers have studied these processes using different techniques and materials; as a result, many parameters affecting both materials and results have been measured. The significant development in this area has been due to the broad range of technological applications including micro/nanofabrication, thin film deposition, ion implantation, etc [2–4]. These processes require ion beams with a suitable degree of ionization and well characterized kinetic energy distributions (KEDs) in the sub-keV or keV range, since these both affect penetration and deposition in the solid [2, 5]. However, the fundamental mechanisms involved in the dynamics of these plasmas remain only partly understood.

In the nanosecond laser pulse regime and for low laser fluences (but nevertheless higher than the ablation threshold), all the mechanisms leading to plasma formation are of a thermal nature. Laser–metal interaction produces a heating of the conduction band electron population; thermal equilibrium in electrons can be assumed due to their fast thermalization times (100 fs). These hot electrons soon relax to the network by electron–phonon scattering processes with times in the picosecond range. The process produces a rapid network heating, melting and evaporation and at moderate fluences drives a phase explosion leading to emission of an overheated gas front, as well as clusters, liquid droplets and large solid fragments. This gas front can be heated by the still existing laser pulse, so that it undergoes thermal ionization. Ionization can also be produced by non-resonant multiphoton absorption, producing a plasma seed (plasma ignition) that couples with the laser and is heated by inverse bremsstrählung [6, 7], strongly

increasing the plasma temperature, and producing further thermal ionization up to the observed high charge states. Temperatures in these plasmas can reach values of tens of eV [8] with power densities of around 10^{10} W cm^{-2}, high enough to produce charges up to +5. Experimental observations show that the expansion of this plasma to vacuum produces a fast multicharged front with suprathermal kinetic energies. The mechanism responsible for this non-thermal ion acceleration is double layer (DL) formation at the plasma–vacuum boundary [9]. Quasi-neutrality is broken in the plasma boundary, so it becomes strongly polarized while the plasma core remains quasi-neutral. The high electric field developed inside this DL drives an 'ion extraction' from the quasi-neutral core and accelerates ions up to the observed suprathermal energies. The quasi-neutral core coexists with the neutral gas reservoir in expansion for a long time after the laser pulse has ended, and is the subject of cooling, decreasing the degree of ionization. Ionization mechanisms are 'frozen' for fast ions due to their extraction from the dense core, otherwise the cooling due to the expansion and radiation losses would not allow the survival of such high charge states. Thermal energy of electrons is transformed into drift energy of the ions; electrons are therefore cooled to accelerate ions. Nevertheless, the laser pulse acts as an energy reservoir keeping or even increasing electron temperature as long as the pulse lasts [10–13].

It is of paramount interest to continue efforts to solve the exact dynamics of these mechanisms as well as to answer many questions that remain open. For instance, it is unclear if the nature of the plasma ignition is purely thermal or photophysical or at what time it takes place. Furthermore, plasma/laser coupling mechanisms are of critical importance as the laser is the energy source of the system. It is nowadays accepted that inverse bremsstrählung is the main mechanism of plasma heating in this density regime, but it is still necessary to obtain real '*in situ*' bremsstrählung cross-sections to measure the efficiency of this process and thus the energy income to the system.

The mechanism of ion acceleration is the DL, and the key parameters of the problem are the plasma density profile, the degree of ionization (i.e. amount of neutrals, and each of the ionic species) and the plasma temperatures (ions and electrons have very different temperatures) [9, 14]. All of these parameters are of course highly time dependent, so any type of experiment that offers time-resolved information about them is welcome.

One of the possible approaches to this type of study is the pump–probe or double-pulse (DP) scheme. This technique, in different configurations, is very useful to check intermediate states following the final state as a variation of the delay between both pulses. DP techniques for plasma studies were initially used in laser-induced breakdown spectroscopy (LIBS) experiments obtaining very interesting results and showing how yields of several spectral lines could be strongly increased by carefully fitting the interpulse delay [7, 15, 16]. Collinear and orthogonal configurations have been used showing that, at suitable delays, the probe laser pulse selectively improves the emission of certain lines in relation to signals obtained in single pulse (SP) experiments. However, these studies are restricted to delay times of microseconds in order to avoid continuum emission due to bremsstrählung and free electronic recombination [7, 16].

The interaction of nanosecond laser pulses on Sn ions produced by a 130–600 ps prepulse has been investigated and the mechanism responsible for changes in the ion kinetic energy discussed in terms of interaction of the delayed pulse with the preplasma [17–19]. Ultrafast DP techniques allow an examination of the emitted optical signals that characterize the target and species escaping from the target, namely ions, neutrals and nanoparticles of great interest in material deposition [20–22]. Adaptive control of the temporal shape of incident laser pulses has also been used to obtain controllable low-energy, high-flux ion beams [23].

Experimental studies on the effect of delayed nanosecond laser pulses on the energy distribution of nanosecond laser-produced plasmas have received little attention, mostly for LIBS purposes. Observing KEDs with a DP scheme is a straightforward step towards an understanding of the overall dynamics of these plasmas, as the final kinetic energies are directly related to the DL dynamics. This paper is a first approach to this study.

Our main type of observation is the KED of ions, but in parallel and as a secondary observation, we have made time-of-flight (t.o.f.) measurements with an ion probe placed along the expansion axis. The ion-probe method employed provides very quick measurements of the overall signal, giving information about the average kinetic energy of the fast ion front. In addition, the interest of these experiments is also to quantify the transmission of the probe laser radiation through the plasma plume in the visible spectral region at different delay times. These measurements have only been partially done in the UV and IR spectral region [7, 12, 13].

In the first part of this work we introduce some DP results of t.o.f. signals from the ion probe. Then DP full KEDs at different interpulse times are presented and compared with the simultaneously obtained ion-probe t.o.f. signals. We analyse the effects of a second pulse upon the plasma created by the first one by means of energy distributions and relative amounts of ions at different interpulse delays. The study has been extended to Al, Cu and Co targets showing similar results, so that the discussion of results is the same for these materials.

2. Experimental

Figure 1 shows the experimental set-up used in this work.

The 532 nm output of two collinear Nd : YAG laser beams, 5 ns FWHM, were focused by a biconvex lens ($f = 500$ mm) onto metallic targets located in a stainless-steel chamber (background pressure 5×10^{-7} mbar). The incidence angle was 30° from the target normal. Laser intensities were measured with a power-meter and varied up to 10 J cm^{-2} (total dual pulse energy) with a set of polarizer and half-wave plate crystals placed at each of the laser beams. A delay generator (BNC, Mod. 555, 0.5 ns timing jitter) launched the timing sequence to run laser flashlamps and Q-switches and at the same time controlled the delay time between both laser pulses. A fast photodiode triggered the detection systems and simultaneously

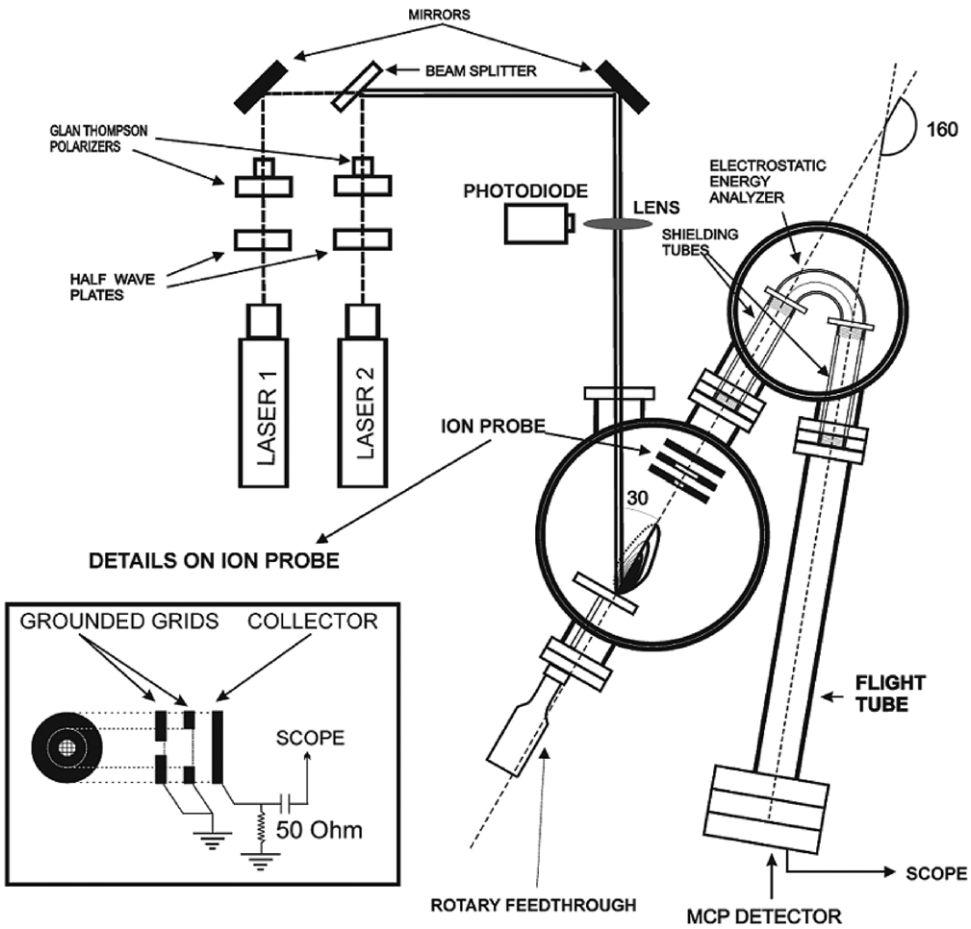

Figure 1. Experimental set-up. The ion probe and EEA used in this work are sketched. Details on the ion probe are also shown. The ion collector can be retracted to allow ions fly freely towards the EEA after passing through grounded grids (see text).

provided control over the delay time between laser pulses. Shot-to-shot fluctuations of laser energies were less than 3%. Photosensitive paper and crater measurements were used to determine the focal spot (diameter of 0.5 mm) and to verify optimal overlapping between laser beams. Samples were rotated so that a fresh surface was continuously exposed to laser pulses which were produced at 1 Hz frequency. Spectra were averaged over 10 shots.

Ions emitted from the target were analysed by two systems: an ion probe and an electrostatic energy analyser (EEA). Both systems were placed alternately along the normal to the target with different objectives as we discuss below. Details in figure 1 show the position and design of the ion probe which consist of a set of two high transmission grids (diameter 1 and 2 cm) facing the target and a copper collector. The distance target–collector was 15 cm long. Grids were formed by a mesh of copper wires and spaced 2 cm one from another. During operation both collector and grids could be used as collectors to test t.o.f. linearity; in this configuration signals at collector and grids have similar shapes, but are most intense in the collector plate due to its higher detection surface. In addition, the first grid is more affected by the perturbations at zero time (laser arrival), which sometimes (depending on laser intensity) can be extended to several microseconds. The physical origin of this perturbation is still controversial, but it seems to be clear at least that it is formed by a complex RF pulse emitted by the plasma and a photoelectron peak [24].

In this work both grids were grounded. They provide t.o.f. measurements of the ion flux in a field free configuration which, consequently, reduces field penetration effects.

In order to measure the KEDs, the collector was retracted allowing charged particles to pass to the EEA (Comstock AC-901) placed in a second vacuum chamber (10^{-8} mbar). A shielding tube avoided the distortion of the ion trajectory due to the EEA external fields. When a potential (ΔV) is applied to hemispherical plates of the EEA, the trajectories that match both the entrance and the exit slits follow this energy/charge ratio:

$$\frac{E}{Z} = 2.25 \times \Delta V. \quad (1)$$

The ions whose trajectories match both of the slits can reach a multichannel plate (MCP) placed at the end of a tube of flight 73 cm long. We assume similar detection efficiency for all ions and energies. Thus, when voltage is applied to the EEA, one obtains a discrete t.o.f. spectrum with as many peaks as charge states existing in the plasma that match the former E/Z ratio. By scanning ΔV and after peak integration, full ion KEDs are obtained. As is well known, the relative energy resolution of the EEA ($\Delta E/E$) depends only on geometric factors [25] which were fixed in this work.

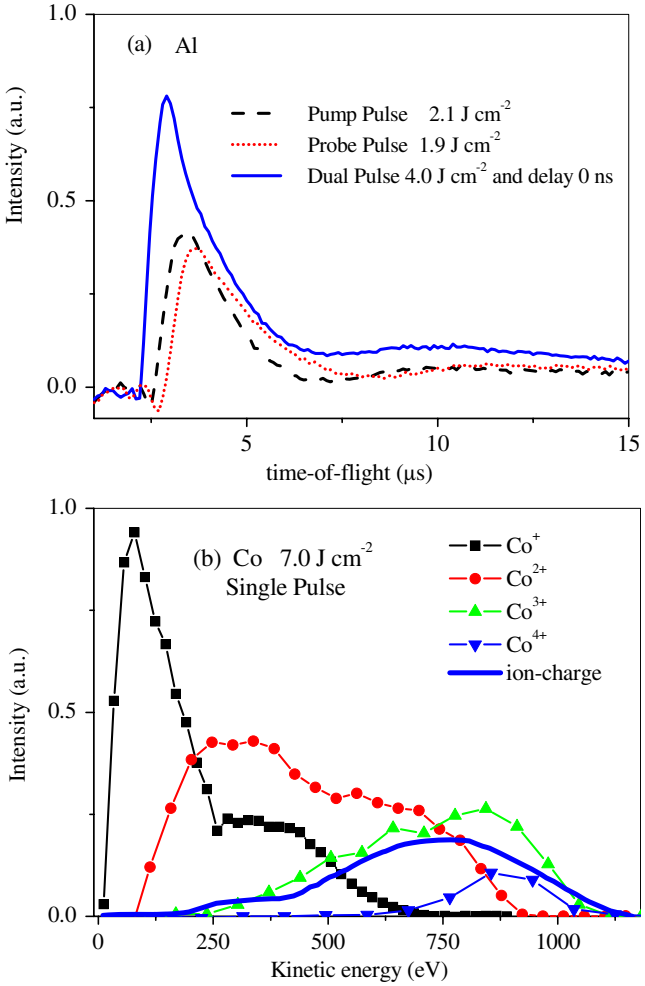

Figure 2. (*a*) T.o.f. signal in the ion collector in DP (solid blue line) and SP experiments (dashed black and short-dotted red lines) with aluminum as target; (*b*) example of KEDs measured in a SP experiment at 7.0 J cm^{-2} of laser fluence and cobalt as target, the ion-charge trace from the ion collector is also shown (see the text).

Figure 2 shows typical signals obtained from the two experimental systems with targets of aluminum and cobalt and 0 ns of delay between laser pulses. Figure 2(*a*) represents the ion colletor t.o.f. signal at laser intensities of 2.1 and 1.9 J cm^{-2} and delay 0 ns. The figure also shows the signal produced by each of the lasers independently (single pulsed experiments) in the dashed black and short-dotted red lines. These energies are lower than the total laser energy used in the dual pulse experiment, and consequently signals are displaced to higher t.o.f.s. Moreover, we have shown that similar t.o.f. traces are obtained in single and dual pulse experiments only if total fluences equal (4.0 J cm^{-2}) and both pulses overlap adequately. In t.o.f. signals, only the time of arrival of the main ion front, or of two fronts if they are observed very clearly, is used as valuable data.

Furthermore, an example of KEDs obtained with the EEA system in a SP experiment is shown in figure 2(*b*). The target was cobalt and the laser fluence was 7.0 J cm^{-2}. Distributions for Co^{+} to Co^{4+} are shown. One can see clearly that ion kinetic energy depends on the charge state. The ion collector signal is charge sensitive and current proportional to the ion charge. Hence, the part of the signal collected at low t.o.f., which corresponds to the arrival of higher charged ions, shows the higher intensity.

Simultaneous measurements of t.o.f. with the ion probe and KED can be obtained removing the charge collector to let the ions pass to the EEA chamber, but using the second grid as charge collector. These t.o.f. signals show low intensities because they are produced at the grid. However, their shapes are identical to the signals obtained in the ion collector and are very useful for discussion purposes as they provide comparisons between both types of measurements. Figure 2(*b*) plots the recorded ion-charge t.o.f. signal (blue line) from the transmission grid. The t.o.f. signal was transformed into energy distributions by the following relation [26]:

$$I(t) = I(E) \cdot \frac{\mathrm{d}E}{\mathrm{d}t}. \tag{2}$$

Both systems (t.o.f. and EEA) have different objectives. Hence, while EEA provides the full KED of all the ions, the ion probe provides quick shot-to-shot t.o.f. spectra of the overall ion front thus saving time and material damage. Some authors are working on deconvoluting t.o.f. spectra to obtain KEDs [26]; but a convergence of results has not yet been achieved.

It should be remembered here that distributions are largely fluence dependent, especially at low laser energies (1–5 J cm^{-2}) where ablation thresholds are reached [8, 27]. Hence, laser pulses with different fluence relations were tested.

Measurements were carried out with Al, Cu and Co (Goodfellow Ltd., 99.9% purity at least) samples. After a few tens of laser shots signals were stabilized and routed from a digital scope (Tektronix TDS360) to a computer for storage. Because all materials analysed show the same qualitative behaviour, examples will be selected to illuminate the results.

3. Results

As has been described it is possible to probe laser-produced plasmas with suitably delayed laser pulses. Here we produce results concerning ion kinetic modifications in laser-produced plasmas by the probe laser. Interpulse times varied from 0 ns (fully overlapped pulses) up to some hundreds of nanoseconds. We will first describe the experimental results obtained by means of the ion collector at different laser fluences. Finally, we will comment on the results concerning the signals collected simultaneously from the EEA and the transmission grid.

3.1. T.o.f. measurements

Figure 3 corresponds to ion-probe signals of aluminum plasma obtained with two pulses of almost equal intensity 2.0 J cm^{-2} at different delays (blue lines).

DP signals for delays from 0 to 200 ns are shown. SP results for each laser independently are also plotted (dashed black and short-dotted red lines). SP produces a signal with only one strong ion peak at 3.7 μs, corresponding to the maximum energy of the ion front that dual experiments

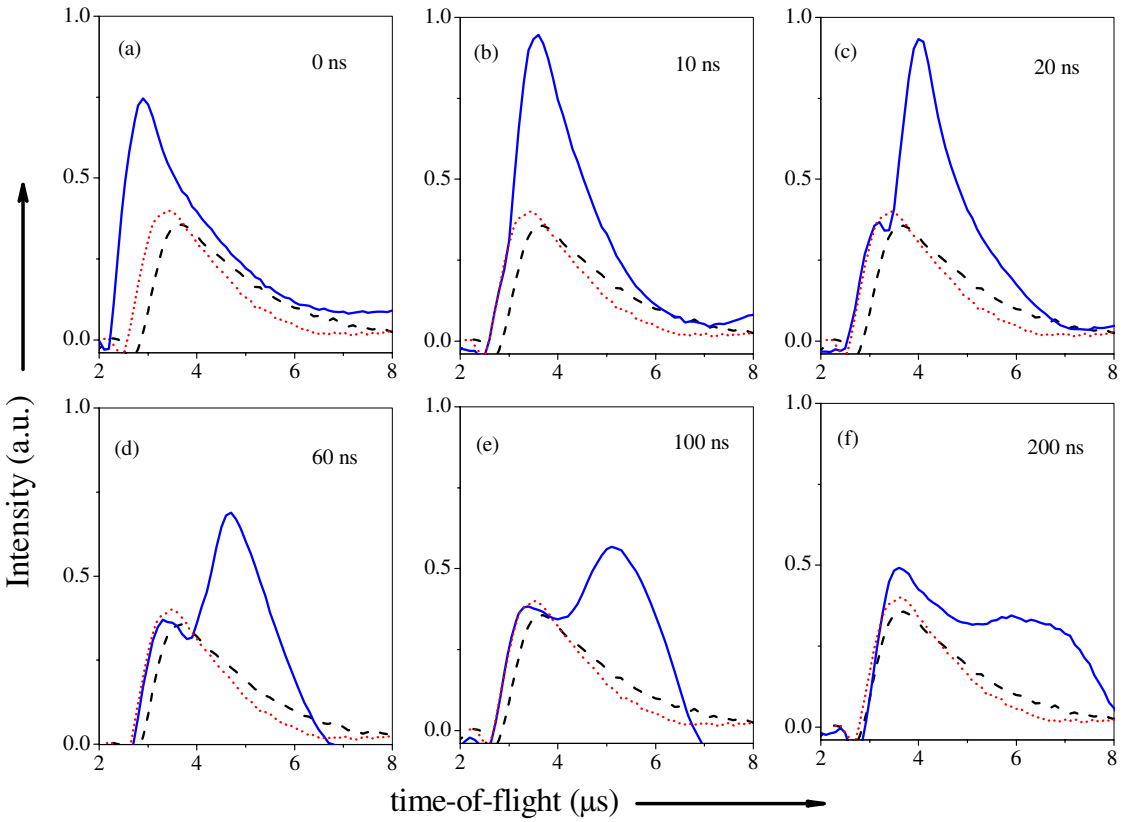

Figure 3. T.o.f. traces collected from the ion probe in DP experiments (solid blue lines) at interpulse times of 0 ns (*a*), 10 ns (*b*), 20 ns (*c*), 60 ns (*d*), 100 ns (*e*) and 200 ns (*e*). Laser energies for the plasma and probe lasers were 2.0 J cm^{-2} approximately. Dashed black and short-dotted red lines correspond to t.o.f. signals produced for both lasers in SP experiments at these fluences. The target was aluminum.

(ion probe and KED) assign to high charge ions (see below). DP results with delays from 0 to 10 ns show ion-probe signals that are very similar to those of SP experiments, but the peak is shifted (figures 3(*a*) and (*b*)) to lower t.o.f.s (higher energies). The maximum shift is registered at 0 ns and corresponds to 2.9 μs of t.o.f., 145 eV of increased energy with respect to the SP experiment. This shift decreases gradually with delay. At 10 ns the signal starts to split into two ion peaks, one of them stays at high energies and the other at lower energies. The high-energy peak is similar in position and intensity to SP peak and does not depend on interpulse time. However, the low-energy peak depends on delay increasing its time of arrival, which has been measured to be 4 μs, 4.7 μs, 5.1 μs and 6.4 μs at delays of 20 ns, 60 ns, 100 ns and 200 ns, respectively (figures 3(*c*) and (*f*)). The intensity of this second peak decreases with delay while it broadens, and is observed until about 400 ns. Negative delays (change in order for plasma and probe laser pulses) produce a completely symmetric behaviour when identical laser pulses are used.

Figure 4 shows t.o.f. traces obtained in the same DP experiment on aluminum targets but using pulses with different fluences: 3.5 J cm^{-2} and 1.0 J cm^{-2} for the plasma and probe laser, respectively. This fluence relation allows us to study effects induced by a low-energy laser pulse on the plasma produced by a more intense laser pulse. Signals measured from SP experiments at 1.0 J cm^{-2} (short-dotted red lines) and 3.5 J cm^{-2} (dashed black lines) are also plotted, showing the same behaviour (single front) but with intensities and energies according to the laser intensity. SP signals peak at around 5 μs and 3 μs, respectively, extending over a long time range. The DP experiment at 0 ns delay time shows an identical signal to that of the plasma laser alone (3.5 J cm^{-2}) but it peaks at 2.9 μs of t.o.f. with higher intensity.

No changes were observed by increasing the delay to 10 ns. At delays higher than 10 ns the peak splits again into two. The lower t.o.f. peak matches the peak obtained in SP experiments while the higher t.o.f. peak is interpulse delay dependent, appearing at 5.2 μs, 6.4 μs and 9.7 μs when the delay is 20 ns, 40 and 200 ns, respectively. In this case the signal was almost equal to the SP experiment but with a second peak superimposed at higher t.o.f. values (lower energies). Delays higher than some microseconds show signals which agree with the formation of two independent plasmas, the latter being produced after a similar time to the delay at which the probe laser was fired.

The next step was to scan ion traces at negative delays (i.e. using plasma and probe laser with fluences of 1 and 3.5 J cm^{-2}, respectively). Ion traces collected from SP experiments of fluences 3.5 J cm^{-2} (dashed black lines) and 1.0 J cm^{-2} (short-dot red lines) are also shown in figure 5.

At 0 ns of delay time we obtained the same results as before (shown in figure 4(*a*)). However by increasing the negative delay from 0 to 10 ns the peak strongly displaced to higher t.o.f. values, and after 15 ns a peak split was observed. The high-energy peak remained near 3 μs, matching the position

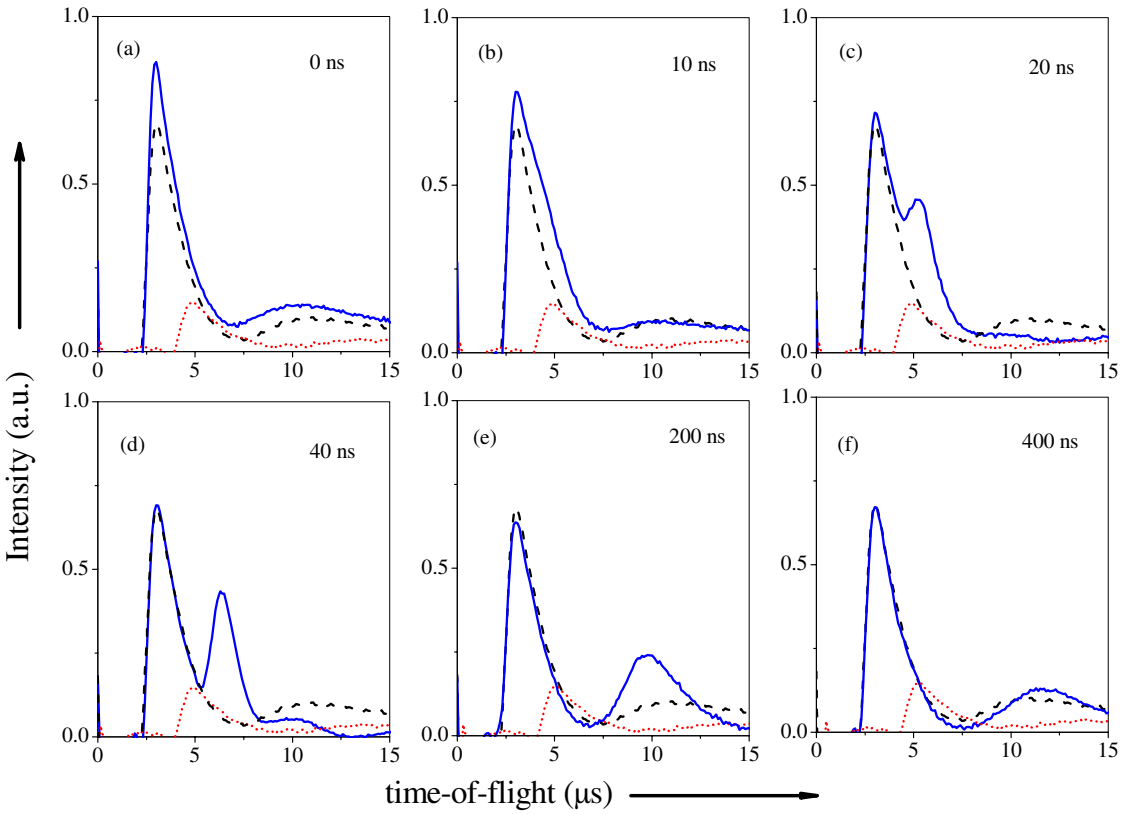

Figure 4. T.o.f. traces collected from the ion probe in DP experiments (solid blue lines) at delays of 0 ns (*a*), 10 ns (*b*), 20 ns (*c*), 40 ns (*d*), 200 ns (*e*) and 400 ns (*f*). Laser energies used to produce the plasma and to probe it were 3.5 J cm^{-2} and 1.0 J cm^{-2}, respectively. Dashed black and short-dotted red lines correspond to t.o.f. signals produced in SP experiments at fluences of 3.5 and 1.0 J cm^{-2}, respectively. The target was aluminum.

of the peak registered by the probe laser in SP experiments while the low-energy one was sensible to the interpulse delay.

3.2. Simultaneous KED and t.o.f. measurements

A straightforward step was to correlate t.o.f. signals with the full ion KED measurements. These studies were carried out by analysing EEA and grid signals when the ion collector was retracted so that ions were allowed to fly to the EEA entrance after passing transmission grids. The transmission grid worked as a pseudocollector.

Figures 6(*b*) and (*f*) show KED obtained in such DP experiments. SP results are also shown in figure 6(*a*).

The target was copper and the fluences for the plasma and probe lasers were equal to 1.5 J cm^{-2}. Figure 6 also plots the simultaneously recorded ion-probe t.o.f. signal (solid blue line) from the transmission grid.

As explained before, it can be appreciated in the SP experiment that the ion-probe single peak is clearly aligned with the maximum energy ion front in the KED, and thus it is composed primarily of +3 and partly of +2 ions.

In DP experiments, at 0 ns of delay (figure 6(*b*)) the energy of the ion front shifts 200 eV in the KED towards higher energies with respect to the SP experiment. Also the mean charge increases. By increasing the interpulse time, the energy shift disappears and the ion front goes back to the energy value and mean charge of the SP experiment. At 15 ns, when the peak split of the ion-probe signal appears, a shoulder structure in the KED arises in the Cu^+ distribution at the same energy (around 290 eV) that the secondary t.o.f. peak. This correlation can be clearly seen at higher delays as the shoulder in Cu^+ increases its intensity and moves to lower energies, perfectly following the low-energy peak of the ion-probe signal (220 eV, 200 eV and 165 eV at delays of 35 ns, 45 ns and 70 ns, respectively). Delays of 35 ns show both the shoulder and the peak starting to decrease in intensity while they continue to move towards lower energies before disappearing. Table 1 summarizes ion velocity variations caused by plasma coupling with the delayed probe pulse.

4. Discussion

Processes triggered from laser–metal interactions with nanosecond pulses have been described by thermal and hydrodynamic models [1–7, 27–29]. The laser energy absorbed is consequently transformed into heat, which is responsible for melting and vaporization (plume formation) of the solid surface. Hence, in the absence of other processes, thermal velocities (u_T) should be observed according to

$$u_T = \sqrt{\frac{8kT_s}{\pi m}}, \tag{3}$$

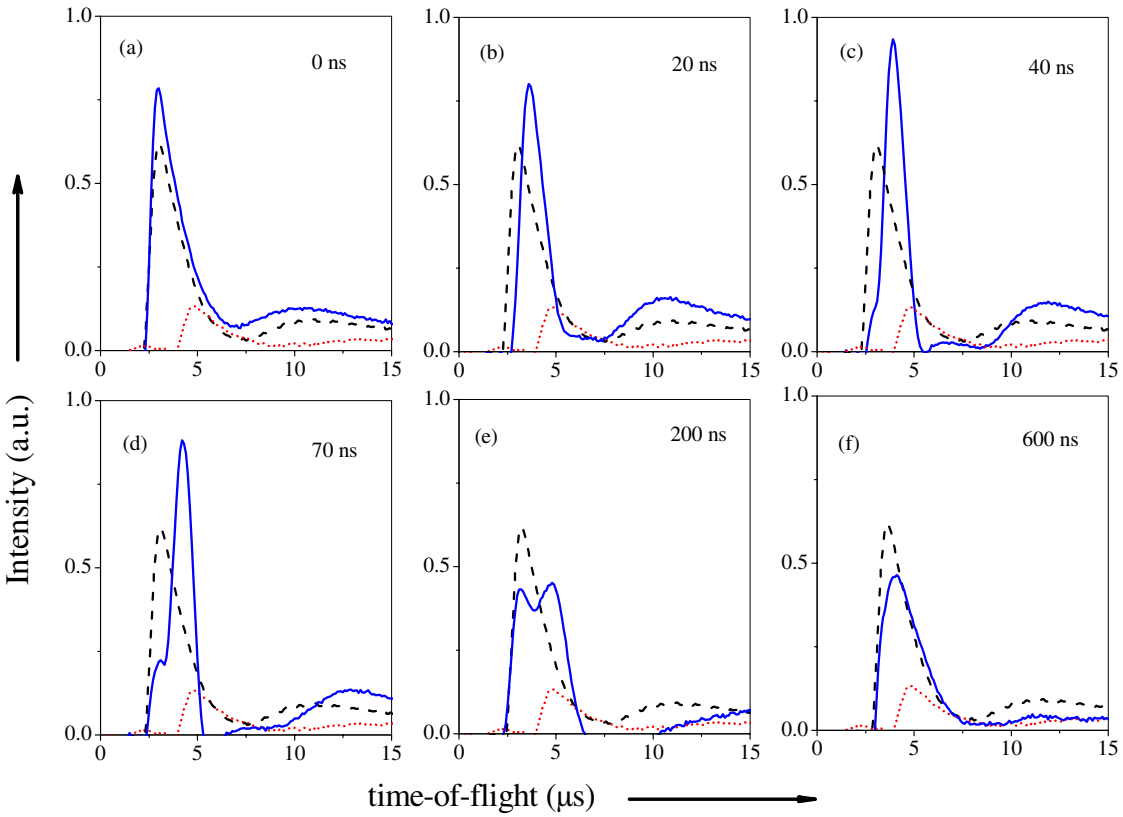

Figure 5. Similar to figure 4 but energies of the first and second laser were 1.0 and 3.5 J cm^{-2}, respectively. Signals at interpulse times of 0 ns (*a*), 20 ns (*b*), 40 ns (*c*), 70 ns (*d*), 200 ns (*e*) and 600 ns (*f*) are shown. The target was aluminum.

where m is the mass of evaporated species and T_s is the surface temperature related to target and radiation properties as

$$T_s = \frac{F(1-R)\alpha}{\rho C_p} \tag{4}$$

where F is the laser fluence, R the reflectivity, α the absorption coefficient of the laser radiation, ρ the density and C_p the heat capacity of the solid [1].

This means that for copper at 1.5 J cm^{-2}, T_s is 1.4×10^4 K with thermal velocities of 2×10^3 m s^{-1}. After 10 ns non-accelerated particles by charge effects have travelled 20 μm, a distance shorter than the laser probe diameter. On the other hand, ion velocities for +2 ions taken from figure 6 reach 2×10^4 m s^{-1}. They travel 10 times the distance of thermal particles. These ions and other high state charges will be out of the region where coupling with the laser probe is produced.

Emission measurements in DP techniques carried out in orthogonal configuration [7] and speed photography [29] have also proved that emission of material from a target is produced in μs time scales in agreement with thermal models. Hence, for DP experiments and concerning nanosecond delays, the probe laser encounters a large amount of vapour.

Experimental results obtained at certain interpulse delays show a different behaviour to that of the SP or to that of the sum of the two independent SP experiment; hence, some kind of coupling is taking place. Moreover, this coupling is delay dependent. The SP results are recovered at delays higher than 600 ns where the coupling disappears completely. It is certainly not irrelevant to discuss whether the two pulse results can be described as a plasma produced by the first one and perturbed by the second one, or whether the contributions cannot be easily separated so that results should be treated as a completely 'new' plasma. We analyse this topic first.

The symmetric experimental results (equal plasma and probe energy pulses) are shown in figures 3 (t.o.f. signal) and 6 (KEDs correlated with t.o.f. signal). The SP experiment produces a t.o.f. signal consisting of one peak followed by signal decay. From the comparison with the SP KED in figure 6(*a*), the peak can be assigned to the high charges and high-energy part of the distribution, while the decay is caused by the low charges and low energies. This can be expected as the ion probe is only sensitive to strong charge fluxes (ion fronts with steep spatial gradients), and the measured current ($j_i(t)$) consists of the superposition of partial currents of ion species $j_i(t) = \sum e \cdot q \cdot v \cdot N_q(t)$, where $v \cdot N_q(t)$ is the stream of ions with charge q [26].

The double-pulse experiment at 0 ns of interpulse delay shows higher energies and charges, in fact the result is similar to a SP experiment of higher laser intensity. As the delay increases, the high-energy part of the distribution gradually matches the SP one while a strong shoulder structure appears in the +1 distribution (which produces the secondary t.o.f. peak). One can suspect that the high-energy part consists of an unaltered, section of the plasma created by the first pulse while the shoulder is a perturbation created by the second pulse. Asymmetric experiments have been performed to shed light on this, as they help to identify and separate the contribution of

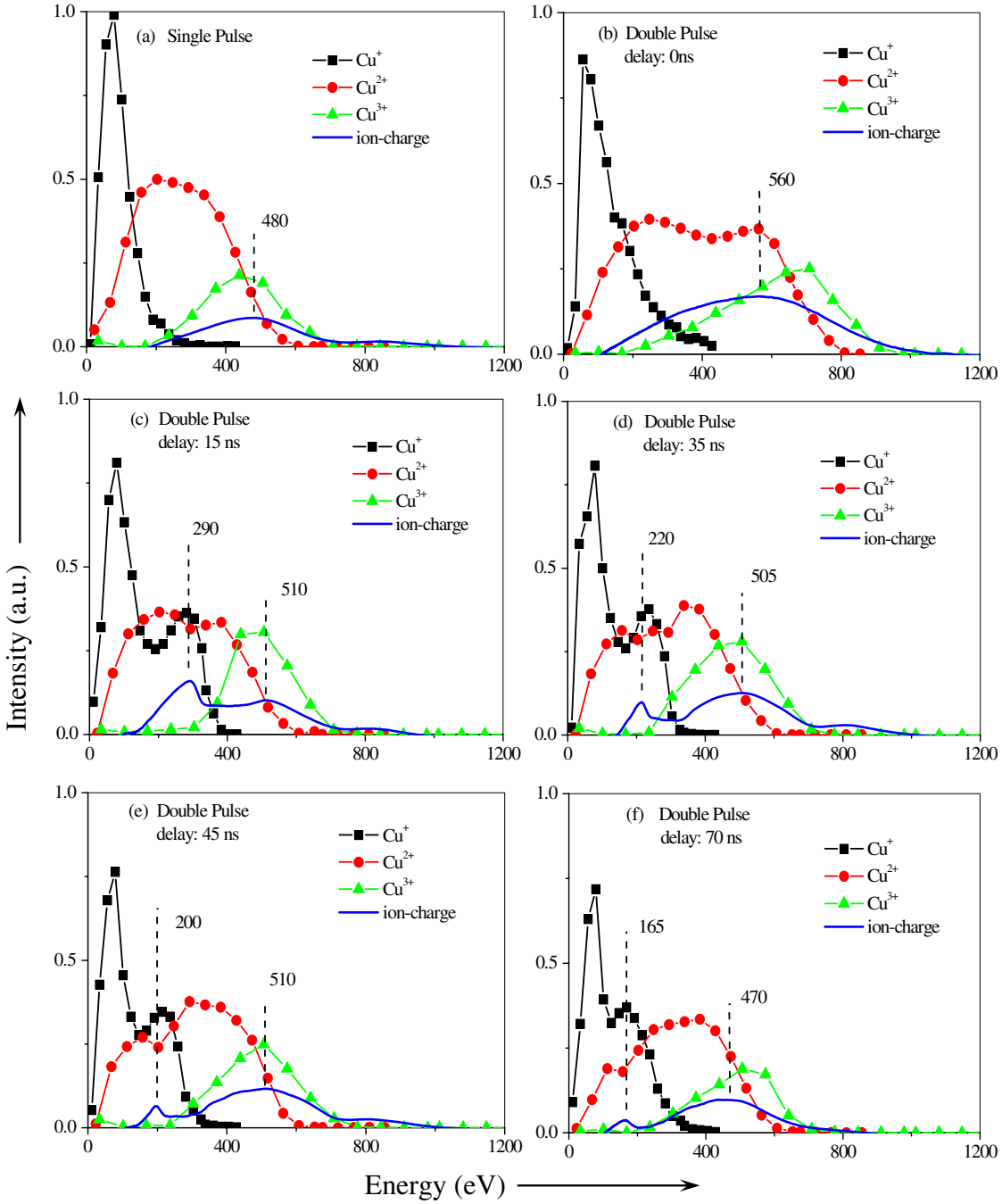

Figure 6. Joint representation of KEDs and t.o.f. traces from the transmission grid (solid blue lines) of ions produced in experiments on copper targets. Laser energies used for plasma production and for probing it were both equal to 1.5 J cm^{-2}. Results in SP mode (*a*) and in DP mode at interpulse times of 0 ns (*b*), 15 ns (*c*), 35 ns (*d*), 45 ns (*e*) and 70 ns (*e*) are shown.

each pulse on the double-pulse results, if it exists. As the total correlation is not symmetrical (i.e. results at negative delays are different from those at positive ones), results help to deduce that two pulse plasmas at delays higher than 10 or −10 ns, keep some key features of the first pulse plasma and present perturbations created by the second one.

Taking this into account, and examining the experiments concerning equal plasma and probe pulses, the results strongly suggest that after 10 ns, the maximum energy and charge state ion front has already been formed and escaped from the interaction zone so that it is no longer perturbed by the second pulse. However, at these delays the second pulse produces a change in the low-energy part of the total distribution. These changes are clear: a secondary ion front appears in the t.o.f. signal (assigned to a shoulder structure in the +1 distribution) and also a 'hole' can be seen in the +2 distribution matching exactly the energy of the +1 shoulder (figure 6). The energy of the second pulse is spent in a totally different manner depending on the conditions that it finds in the interaction region, especially after 10 ns. At this time the second pulse is used up, increasing the number of detected +1 ions and their mean energy. On the other hand, at delays between 0 and

Table 1. Ion peak velocities in t.o.f. traces measured in a double-pulse experiment at different delays. Pump and probe laser were 1.5 J cm^{-2}. The target was copper.

	Velocities (10^4 m s^{-1})		
		Double pulse	
Delay (ns)	Single pulse	High-energy peak	Low-energy peak
0	3.8	4.1	—
5		3.7	—
10		3.4	—
15		3.9	3.0
20		4.0	2.9
25		4.0	2.8
35		3.9	2.6
45		3.9	2.5
55		3.9	2.4
70		3.8	2.2

10, the second pulse contributes directly to the main front, creating an initial plasma of higher temperature, density and charge state.

Several phenomena are expected to take place when the second pulse arrives at the interaction zone: plasma heating, photoionization of neutrals and further sample evaporation. Plasma heating main mechanism at these laser intensities is inverse bremsstrählung. This heating would cause further thermal ionization and an increase of the DL voltage.

Effects of the probe laser on the laser-produced plasma can be understood if we consider that interaction is produced in the quasi-neutral core of the plasma (the region that is not affected by the DL) [17]. If dense plasmas are produced, laser photons will be absorbed and scattered by the plasma, especially if plasma approaches critical density. Plasma shielding effects observed in laser-produced plasmas are a consequence of such high densities [12, 27]. On the other hand, if low density plasmas are produced, more photons from the probe laser will be transmitted through the plasma towards the target surface, causing new plasma formation.

Figure 6 shows that after 10 ns the probe laser basically modifies the Cu^+ ion distribution. This fact is not observed in Cu^{2+} and Cu^{3+} distributions, probably because multicharged ion populations have been depleted in the quasi-neutral core due to the higher acceleration they experienced at early plasma stages. Hence, when the probe laser pulse meets the plasma core , the high charge ions are already out of the probed region.

Furthermore, additional information can be obtained from experiments carried out on high-energy laser-produced plasmas probed by a low-energy pulse (figure 4). These results do not show any transmission of the probe laser because the plasma is too dense and the probe laser energy is low. In spite of this, a group of new ions are produced. We have measured the area under the ion trace produced in SP experiment by the plasma laser and compared with the area derived from DP experiments; this difference is related to new ions created by the probe laser. Moreover, these ions are +1 charged, as we had observed previously in experiments carried out with the EEA and the transmission grid simultaneously (figure 6). In short, the species responsible for +1 ion production are neutrals

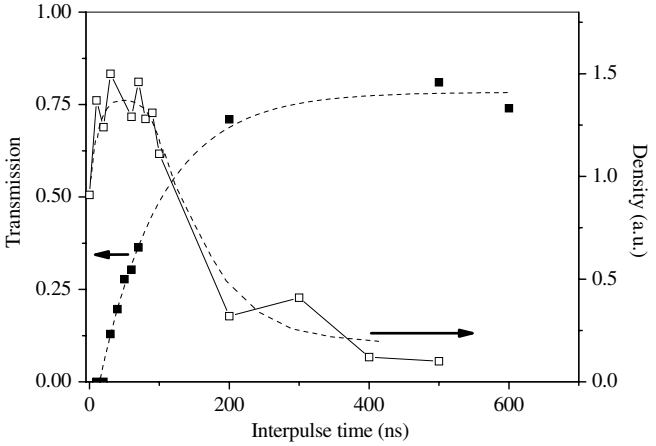

Figure 7. Joint plot of the temporal evolution of density and transmission through a laser-produced plasma of aluminum. Data were extracted from DP experiments shown in figures 4 and 5. Lines are guides to the eye.

and electrons. Electrons considerably increase their energy by inverse bremsstrählung, being responsible for ion production by electron–neutral collisions. Photoionization should also be considered but at a wavelength of 532 nm it shows less influence [6, 7, 10, 11]. In either case, the new group of ions can be related to the number density of species in the plasma and, consequently, with the plasma and/or vapour density.

Experiments carried out to study effects of high-energy probe lasers on low-energy laser-produced plasmas (figure 5) show traces with a new peak appearing around 3 μs at interpulse delays higher than 40 ns. The intensity of the peak increases with delay, matching the trace obtained in SP experiments at interpulse times of some microseconds. It is clear in DP experiments that, as the plume expands, the target becomes more accessible for the production of new plasma by the probe laser. This production is related to the temporal variation of plasma shielding.

Variation in absolute transmission (T) through the plasma can be obtained as the relation between the peak intensity at 3 μs produced by the probe laser at different delays (I_t) and the peak intensity produced by the probe laser in the absence of plasma (I_0), namely in an SP experiment or some μs after the plasma was produced:

$$T = \frac{I_t}{I_0} = \frac{I_0 - (I_{abs} + I_{ref})}{I_0} \qquad (5)$$

where I_{abs} and I_{ref} refer to the absorbed and reflected laser intensity by the plasma plume.

Figure 7 represents simultaneously the transmission through the plume derived from equation (5) and the area of the new group of ions produced by the probe laser at different interpulse times.

Both studies lead us to similar conclusions about the plasma. Maximum values in density are reached a few nanoseconds after the plasma laser, in agreement with a delayed heating of the target in relation to the laser pulse [10, 11]. During the first nanoseconds the plasma is completely opaque to the laser pulse. However, 200 ns after the plasma is

produced, the transmission of the probe laser increases to 70%, while particle density exhibits a slow decrease. Moreover, both behaviours can be fitted to Maxwellian and exponential functions according to previously published models [5, 10].

5. Conclusions

In summary, we have studied the coupling between laser-produced plasmas and probe laser pulses at different interpulse delays in the nanosecond time range. Experiments were performed at 532 nm laser radiation on Al, Cu and Co targets and by means of an ion-probe collector and an EEA-t.o.f. The coupling between the plasma and the probe laser is produced during hundreds of nanoseconds and, depending on plasma and laser energies, different phenomena have been observed. The probe laser arriving at the plasma at interpulse times above 10 ns produces new +1 ions of high energy, while multicharged ions in the plasma are not affected except in the low-energy part of the distribution, where a 'hole' can be observed at exactly the same energy where the +1 shoulder structure appears. This fact can be related to the acceleration experienced by species due to the appearance of a new DL in the dense core (interaction zone) and produced by the probe laser pulse. Consequently, after 10 ns, the high-energy part of the high charges has already been formed and abandoned the core of the plasma. On the other hand, the low-energy part of low charges is influenced at delays of up to hundreds of nanoseconds, depending on the intensity of the plasma pulse.

The coupling of a laser-produced plasma with a second pulse can be used to test the dynamics of plasma formation and expansion in laser-produced plasmas. The results are in good agreement with previous observations and plasma models, which show that maximum temperature and density are reached within the times of the laser pulse. In these experiments, ions should be produced in the first stages, expanding quickly. The rest of the laser pulse undergoes a screening, being partially absorbed by the plasma core, and increasing especially the population of +1 ion.

Further studies, both experimental and theoretical, are in progress to clarify ion formation mechanisms and relation to laser fluences. In particular, we are applying double-pulse techniques to phase explosion time lag studies, which are of great interest in many ion-mixing experiments, primary ion deposition and ion doping in solids. We are also using the 1D particle-in-cell method for the simulation of the DL acceleration on the onset of this dynamics of plasma formation.

Acknowledgments

This work was partly supported by Spanish MICINN through grants CTQ2009-06968 and CTQ2010-17749. The University of the Basque Country UPV/EHU and the Basque Government GV are also thanked for partial support. J.I.A. thanks UPV for a research fellowship.

References

[1] Phipps C R 2007 *Laser Ablation and its Applications* (Berlin: Springer)
[2] Chrisey D B and Hubler G K 1994 *Pulsed Laser Deposition of Thin Films* (New York: Wiley)
[3] Rubahn H-G 1996 *Laser Applications in Surface Science and Technology* (New York: Wiley)
[4] Koudoumas E, Spyridaki M, Stoian R, Rosenfeld A, Tzanetakis P, Hertel I V and Fotakis C 2004 *Thin Solid Films* **453–454** 372
[5] Rosinski M, Badziak J, Czarnecka A, Gasior P, Parys P, Pisarek M, Turan R, Wolowski J and Yerci S 2006 *Mater. Sci. Semicond. Process.* **9** 655
[6] Chen Z and Bogaerts A 2005 *J. Appl. Phys.* **97** 063305
[7] Cristoforetti G, Lorenzetti G, Benedetti P A, Tognoni E, Legnaioli S and Palleschi V 2009 *J. Phys. D: Appl. Phys.* **42** 225207
Cristoforetti G, Legnaioli S, Palleschi V, Salvetti A and Tognoni E 2008 *Spectrochim. Acta* B **63** 312
[8] Apiñaniz J I, Sierra B, Martínez R, Longarte A, Redondo C and Castaño F 2008 *J. Phys. Chem.* C **112** 16556
[9] Bulgakova N M, Bulgakov A V and Bobrenok O F 2000 *Phys. Rev.* E **62** 5624
[10] Lunney J G and Jordan R 1998 *Appl. Surf. Sci.* **127–129** 941
Jordan R and Lunney J G 1998 *Appl. Surf. Sci.* **127–129** 968
[11] Donnelly T and Lunney J G 2008 *Appl. Phys.* A **92** 951
[12] Mao X and Russo R E 1996 *Appl. Phys.* A **64** 1
[13] Schittenhelm H, Callier G, Berger P and Hugel H 1996 *J. Phys. D: Appl. Phys.* **29** 1564
[14] Apiñaniz J I and Martínez R 2011 *IEEE Trans. Plasma Sci.* **39** 2928
[15] Krstulovic N and Milosevic S 2010 *Appl. Surf. Sci.* **256** 4142
[16] Scaffidi J, Angel S M and Cremers D A 2006 *Anal. Chem.* **78** 24
[17] Tao Y, Tillack M S, Harilal S S, Sequoia K L and Najmabadi F 2007 *J. Appl. Phys.* **101** 023305
[18] Rus B, Carillon A, Dhez P, Jaeglé P, Jamelot G, Klisnick A, Nantel M and Zeitoun P 1997 *Phys. Rev.* A **55** 3858
[19] Nakamura D, Akiyama T, Okazaki K, Tamaru K, Takahashi A and Okada T 2008 *J. Phys. D: Appl. Phys.* **41** 245210
[20] Gordillo-Vázquez F J, Perea A, McKiernan A P and Afonso C N 2005 *Appl. Phys. Lett.* **86** 181501
[21] Scuderi D, Albert O, Moreau D, Pronko P P and Etchepare J 2005 *Appl. Phys. Lett.* **86** 071502
[22] Spyridaki M, Koudoumas E, Tzanetakis P, Fotakis C, Stoian R, Rosenfeld A and Hertel I V 2003 *Appl. Phys. Lett.* **83** 1474
[23] Stoian R, Mermillod-Blondin A, Bulgakova N M, Rosenfeld A, Hertel I V, Spyridaki M, Koudoumas E, Tzanetakis P and Fotakis C 2005 *Appl. Phys. Lett.* **87** 124105
[24] Hong M H and Lu Y F 2000 *Appl. Phys. Lett.* **76** 248
[25] Imhof R E, Adams A and King G C 1976 *J. Phys.* E **9** 138
[26] Krása J, Jungwirth K, Krouský E, Láska L, Rohlena K, Ullschmied J and Velyhan A 2008 *Radiat. Eff. Defect. S.* **163** 419
[27] Amoruso S, Armenante M, Berardi V, Bruzzese R and Spinelli N 1997 *Appl. Phys.* A **65** 265
[28] Dreyfus R W 1991 *J. Appl. Phys.* **69** 1721
[29] Geohegan D B 1992 *Appl. Phys. Lett.* **60** 2732